JCB

Urbina et al., https://doi.org/10.1083/jcb.201709064

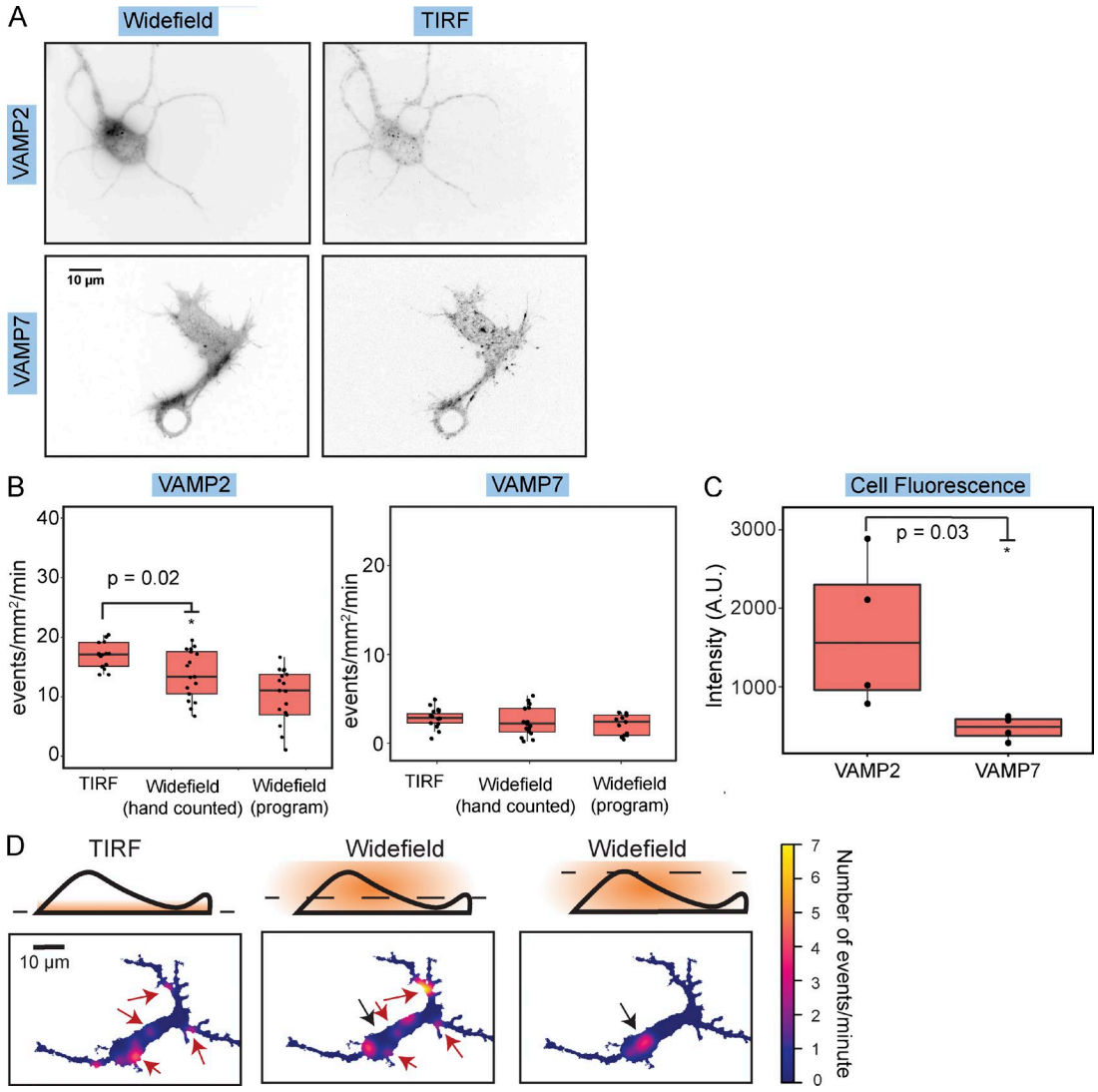

Figure S1. **Widefield and TIRF imaging of VAMP2-pHluorin and VAMP7-pHluorin. (A)** Single images from widefield and TIRF time lapse microscopy of cortical neurons expressing either VAMP2-pHluorin or VAMP7-pHluorin 48 h in vitro. **(B)** Box and whisker plots of the frequency of VAMP2-pHluorin and VAMP7-pHluorin exocytosis measured from TIRF and widefield imaging (n = 17 cells for VAMP2, n = 14 cells for VAMP7; box represents median ± IQR, whiskers reach the minimum and maximum values within 1.5 times the IQR). **(C)** Box and whisker plots of the background plasma membrane fluorescence levels measured from widefield images of VAMP2-pHluorin– and VAMP7-pHluorin–expressing neurons (n = 4 per condition). **(D)** Heat maps of density of VAMP2-pHluorin exocytosis observed by TIRF (left) and widefield microscopy at bottom (middle) and top (right) focal planes. Black arrows demarcate how apparent exocytic frequency detection changed with the focal plane. Pink arrows denote clusters apparent by TIRF and at the lower focal plane in widefield that were absent in the higher focal plane in widefield images.

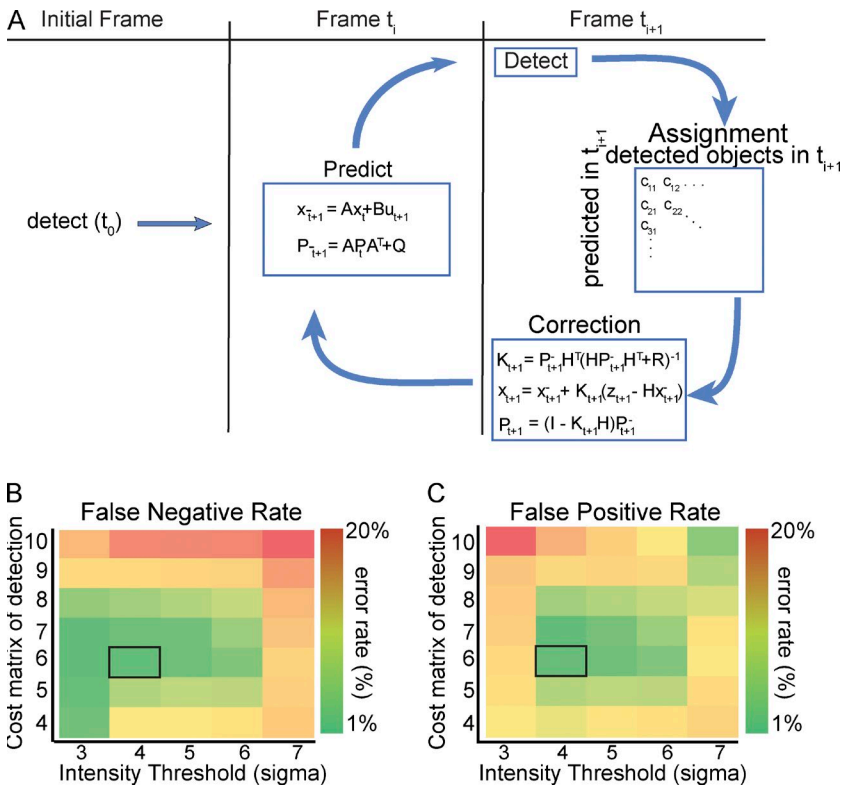

Figure S2. **Kalman filter algorithm and parameter selection. (A)** Schematic of the Kalman filter used for linking potential exocytic events between frames. X is defined as a state vector of the object (position and velocity), P is the covariance matrix of X, A is the prediction matrix, B is the control matrix, u is the control vector, Q is an added noise covariance matrix, H is the measured position of an object, R is the covariance modeling the uncertainty of the measured position of an object, Z is the measured position of an object, and K is the Kalman gain. "c" represents the Euclidean distance "cost" between two objects in the cost matrix. To recognize whether objects detected in multiple frames are the same or different objects, the Kalman filter predicts the location of current objects in the subsequent frame. Fluorescent objects were detected in the first frame (t_0). Using a prediction function, which took into account velocity and current location of the detected fluorescent object, the location of each object was predicted for the next frame (t_{+1}). The prediction function was initialized with an experimentally determined set of parameters. After the prediction was made, fluorescent objects were detected in the next frame (t_{+1}). These detected objects were then assigned either as a new object, or as a previously detected object based on a cost matrix, which assigned a cost between the distance of predicted locations of objects and detected objects. The penalties assigned to this cost matrix were determined experimentally (B and C). After the newly detected objects were assigned, the prediction function was corrected based upon the error between predicted object locations and detected object locations. The cycle was then repeated, predicting the next location of objects in frame t_{+2}. **(B and C)** Cost matrices of the false-negative (B) and false-positive (C) rates of event detections with using varying intensity thresholds for detecting events. This indicates how high the signal-to-background ratio must be for pixels to be recognized as a potential exocytic event. False-positive rates were computed as 100 × (1 − M/D) and false-negative rates as 100 × (1 − M/G), where D is the number of computer-detected exocytic events, G is the number of user-defined detected exocytic events, and M is the number of matches between the two, as described in Matov et al. (2010).

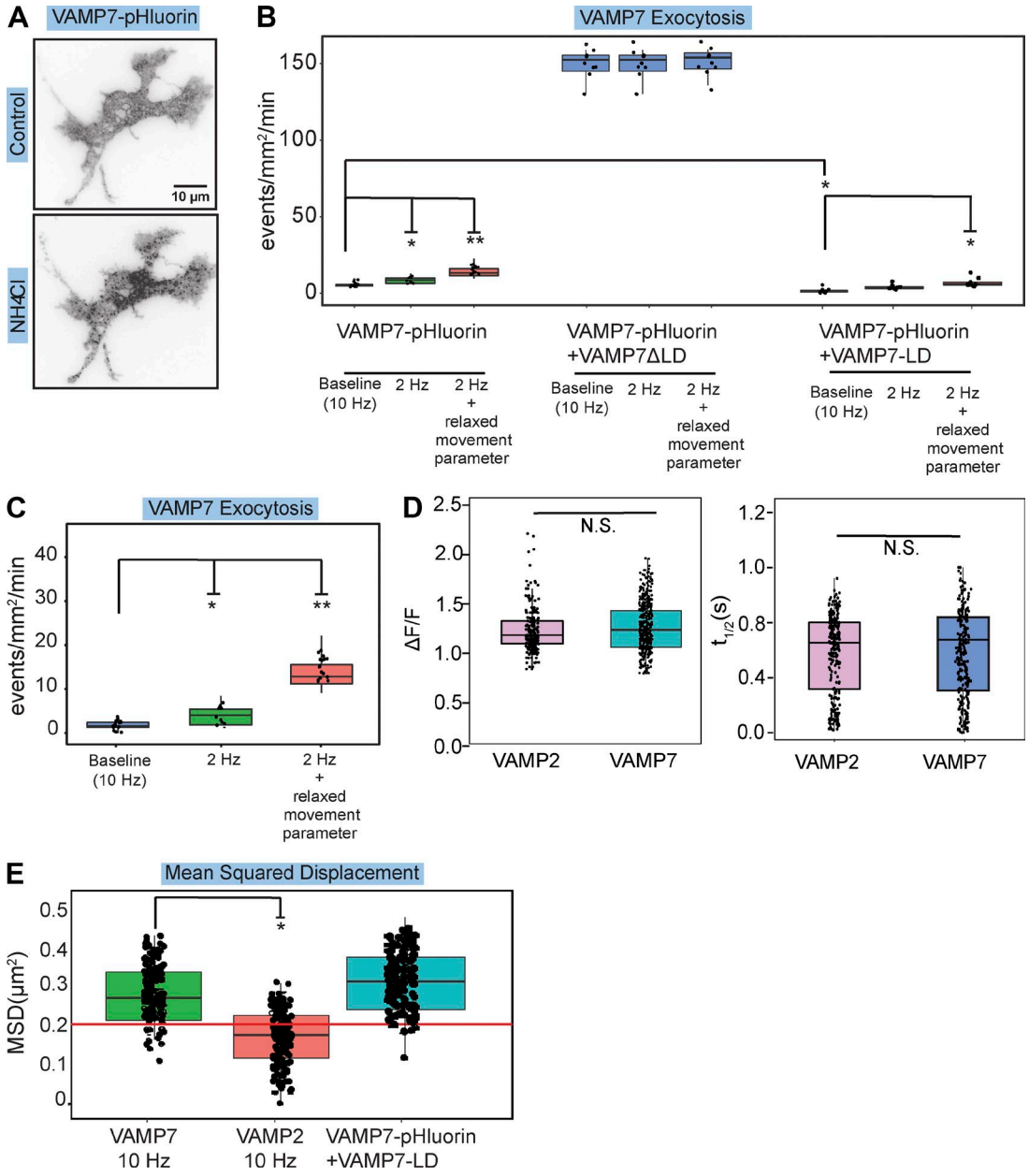

Figure S3. **Confirmation of VAMP7-pHluorin exocytosis. (A)** Example minimal projections of TIRF time-lapse images of VAMP7-pHluorin before and after treatment with NH_4Cl. **(B)** Box and whisker plots of detected frequency of exocytosis of VAMP7-pHluorin, VAMP7-pHluorin + VAMP7ΔLD, or VAMP7-pHluorin + VAMP7-LD at different acquisition rates and different movement parameter thresholds (n = 9 cells per condition; box represents median ± IQR, whiskers reach minimum and maximum values within 1.5 times the IQR). **(C)** Box and whisker plots of the detected frequency of VAMP7-pHluorin exocytosis at baseline (10 Hz), at 2 Hz, and at 2 Hz with the movement parameter threshold of detection relaxed (n = 14, P = 0.02 between baseline and 2 Hz, P = 0.001 between baseline and 2 Hz + relaxed movement parameter). **(D)** Box and whisker plots of the change in peak fluorescence (left) and $t_{1/2}$ (right) of VAMP2-pHluorin– and VAMP7-pHluorin–mediated events (n = 562 for VAMP2, n = 578 for VAMP7). **(E)** Box and whisker plots of the mean squared displacement (MSD) of potential exocytic events (n = 343, 366, 378 for VAMP7, VAMP2, and VAMP7+VAMP7-LD, respectively). The red line indicates the experimentally produced threshold, based on the diffraction-limited resolution of the microscope. *, P < 0.05; **, P < 0.01.

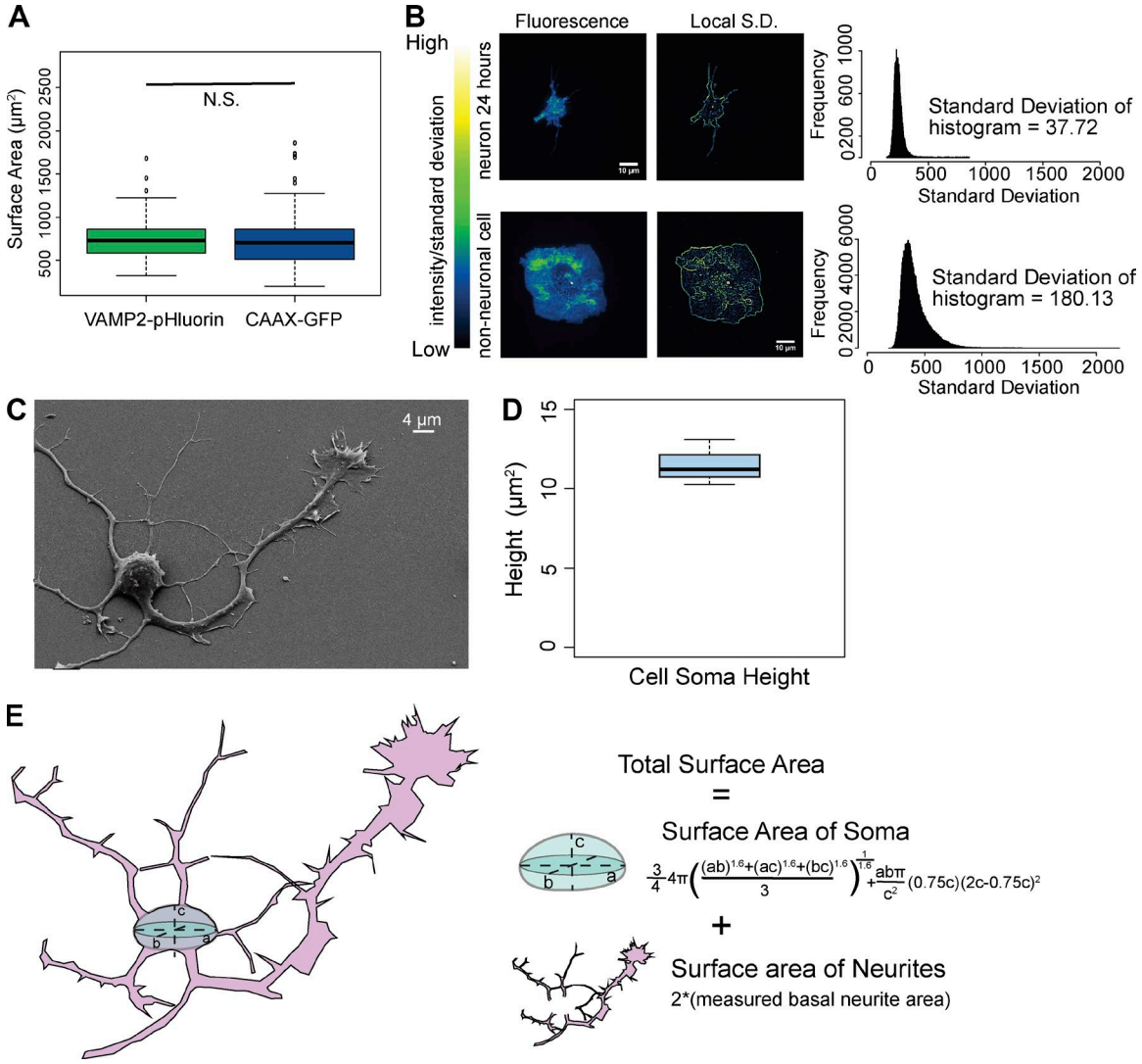

Figure S4. **Estimation of membrane surface area of neurons. (A)** Box and whisker plots of surface area calculated from both VAMP2-pHluorin– and CAAX-GFP–expressing neurons at 24 h in vitro (n = 62 for VAMP2-pHluorin, n = 63 for CAAX-GFP; box represents median ± IQR, whiskers reach minimum and maximim values within 1.5 times IQR). **(B)** Left: Fluorescence intensity and local SD of cells with and without visible membrane folding. Right: histogram of local SD of pixels of each of cell (n = 69,074 pixels for neuronal cell, n = 227,639 pixels for nonneuronal cell). SD of the spread of local SDs of the cell is noted. **(C)** Scanning electron micrograph of neuron at 48 h in vitro. **(D)** Box and whisker plot of the measured height of neuron somas at 48 h in vitro (n = 15). **(E)** Surface area estimation of neurons, with separate estimations for the neurite and soma.

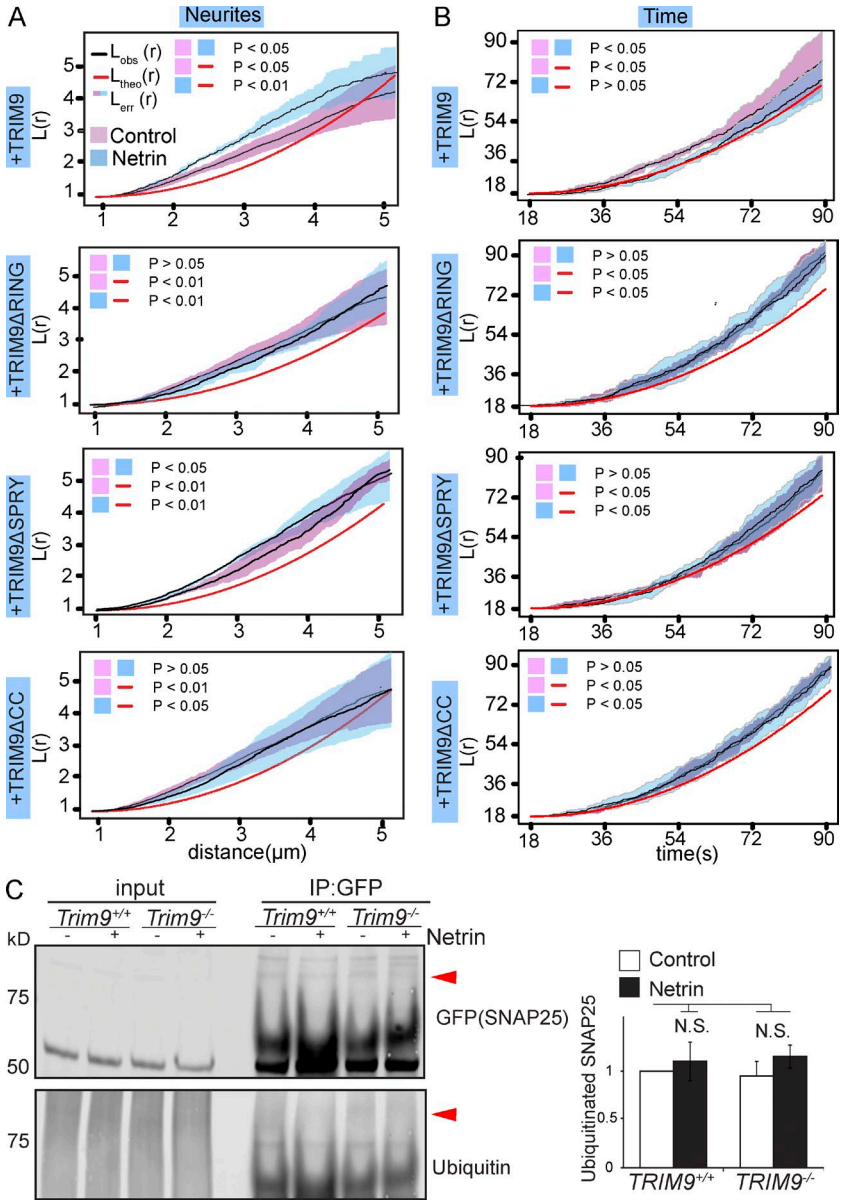

Figure S5. **Specific domains of TRIM9 modulate distinct parameters of exocytosis in neurites. (A and B)** 1D Ripley's L(r) function of spatial distribution in neurites (A) and temporal distribution (B) of exocytosis of *Trim9*$^{-/-}$ mouse cortical neurons expressing the indicated TRIM9 domain mutant. Expression of TRIM9 rescued netrin-1–dependent spatial clustering in neurites and netrin-1–dependent temporal relaxation of exocytic clustering lost in *Trim9*$^{-/-}$ neurons. The RING and CC domains of TRIM9 were required to rescue the netrin-dependent spatial clustering (n = 16 for each condition). **(C)** SDS-PAGE and Western blot of inputs and GFP-SNAP25 immunoprecipitates from *TRIM9*$^{+/+}$ and *TRIM9*$^{-/-}$ HEK293 cells immunoblotted for GFP and ubiquitin. High molecular mass ubiquitin in the immunoprecipitate is considered SNAP25 ubiquitination (arrowheads). Plot shows mean values of SNAP25 ubiquitination ± SEM (n = 3). Ubiquitination of SNAP25 did not change significantly in the absence of *TRIM9* or the presence of netrin-1. P values calculated from Kruskal-Wallis ANOVA followed by least significant difference post hoc correction compared with *TRIM9*$^{+/+}$ control.

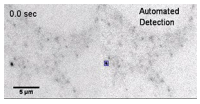

Video 1. **Identification of exocytic events.** Left: Inverted contrast images of E15.5 cortical neuron cultured for 48 h in vitro expressing VAMP2-pHluorin were acquired every 100 ms by TIRF microscopy with 110-nm penetration depth to visualize VAMP2-mediated exocytosis, which is marked by a rapid increase, followed by diffusion and decrease in fluorescence intensity. Right: The same time-lapse is overlaid with detected fluorescent events that meet the criteria of exocytosis events (red): nonmotile, transient (appears and disappears during course of imaging), diffraction-limited fluorescent events that reach peak fluorescence in the first frame (t_0) and decay exponentially over subsequent frames (t_{+i}), and detected events that fail to reach these criteria (blue).

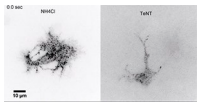

Video 2. **Confirmation that detected exocytic events are bona fide.** Inverted contrast images of E15.5 cortical neuron cultured for 48 h in vitro expressing VAMP2-pHluorin were acquired every 100 ms by TIRF microscopy with 110 nm penetration depth to visualize VAMP2-mediated exocytosis, which is marked by a rapid increase, diffusion, and decrease in fluorescence intensity. Left: Treatment with NH_4Cl alkalinizes intracellular compartments, reversing the quenching of VAMP2-pHluorin and making VAMP2-pHluorin–containing vesicles fluorescent before fusion pore opening. Right: TeNT treatment, which cleaves the cytoplasmic face of VAMP2, blocks SNARE complex formation and VAMP2-mediated exocytosis.

Video 3. **VAMP2-mediated exocytosis changes over developmental time.** Inverted contrast images of E15.5 cortical neurons cultured for 24 (left), 48 (middle), and 72 h (right) in vitro expressing VAMP2-pHluorin were acquired every 100 ms by TIRF microscopy with 110-nm penetration depth to visualize VAMP2-mediated exocytosis. Blue squares indicate tracked objects. Red squares indicate automatically detected exocytic events.

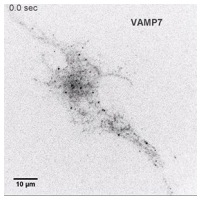

Video 4. **VAMP7-mediated exocytosis adds negligible amount of membrane.** Inverted contrast images of E15.5 cortical neurons cultured for 48 h in vitro expressing VAMP7-pHluorin were acquired every 100 ms by TIRF microscopy with 110-nm penetration depth to visualize VAMP2-mediated exocytosis.

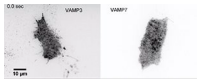

Video 5. **VAMP3- and VAMP7-mediated exocytosis in VMM39 melanoma cells.** Inverted contrast images of interphase VMM39 melanoma cells expressing VAMP3-pHluorin (left) and VAMP7-pHluorin (right) were acquired every 500 ms by TIRF microscopy with 110 nm penetration depth to visualize VAMP-mediated exocytosis, which is marked by a rapid increase, diffusion, and decrease in fluorescence intensity.

Provided online a ZIP file containging macros. Run_script.m runs the entire detection algorithm over a folder of image stacks. Cell_mask.m creates a binary mask of a cell from a fluorescent image. Detection_algorithm.m finds all possible exocytic events and fluorescent puncta in each image of a z-stack. Multiobject_tracking.m performs the Kalman filter function, linking fluorescent events across frames and throwing out nonexocytic objects. Extract_fusion.m compiles the fluorescent pixel values, time points, and x and y positions of exocytic events and saves them to a CSV file. Full_fusion_script.R computes features of each exocytic event. Cell_SurfaceArea.R computes the surface area of the cell soma gives the length, width, and height. Bayesian_Cell_Model.R performs linear Bayesian analysis. Spatial_analysis.R performs the Ripley's K function on exocytosis given a list of events and a cell mask.

Reference

Matov, A., K. Applegate, P. Kumar, C. Thoma, W. Krek, G. Danuser, and T. Wittmann. 2010. Analysis of microtubule dynamic instability using a plus-end growth marker. *Nat. Methods.* 7:761–768. https://doi.org/10.1038/nmeth.1493